Supplemental Figures

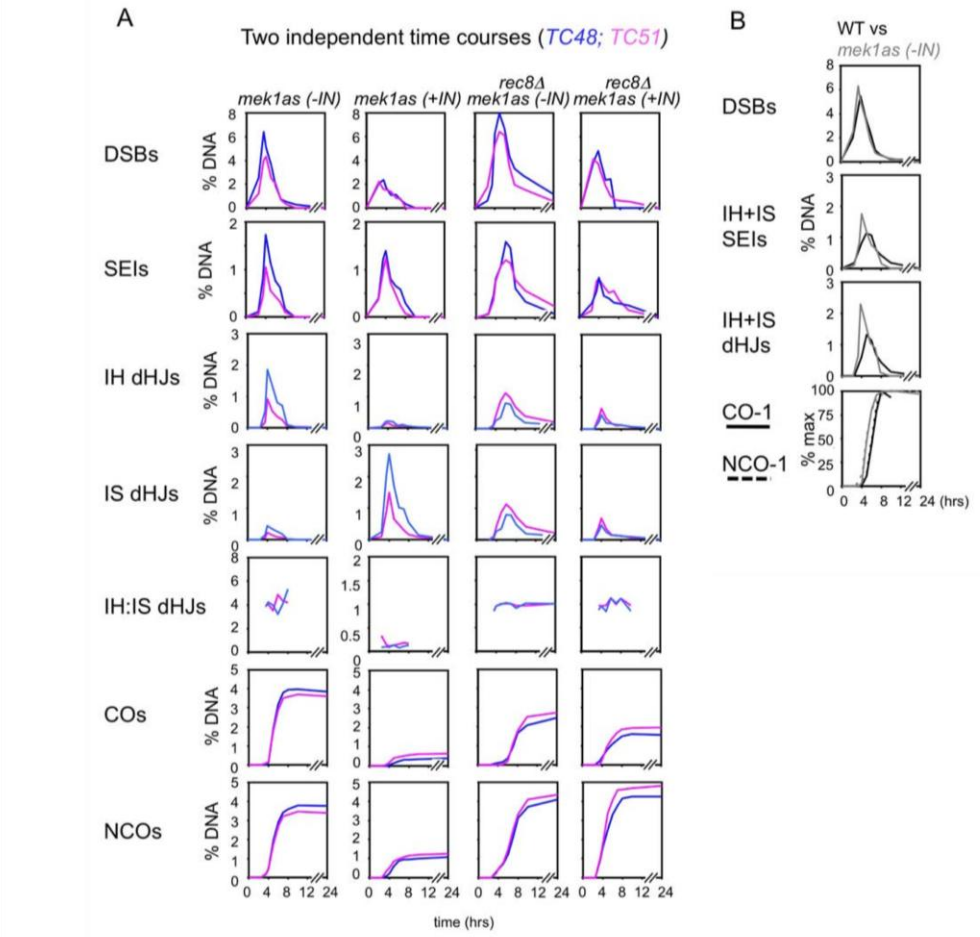

Figure S1. Time course details. Related to Figure 2. (A) Reproducibility of time course data between independent experiments. Two independent time courses, each assaying all four indicated strains in parallel on the same day. These data illustrate (i) reproducibility of primary data from experiment to experiment including reproducibility of IH:IS dHJ ratios; and (ii) constancy of IH:IS dHJ ratios over time in meiosis**.** (B) Comparison of WT and *mek1as(-IN).* The *mek1as(-IN)* allele does not significantly alter recombination in the absence of inhibitor in an otherwise WT background.

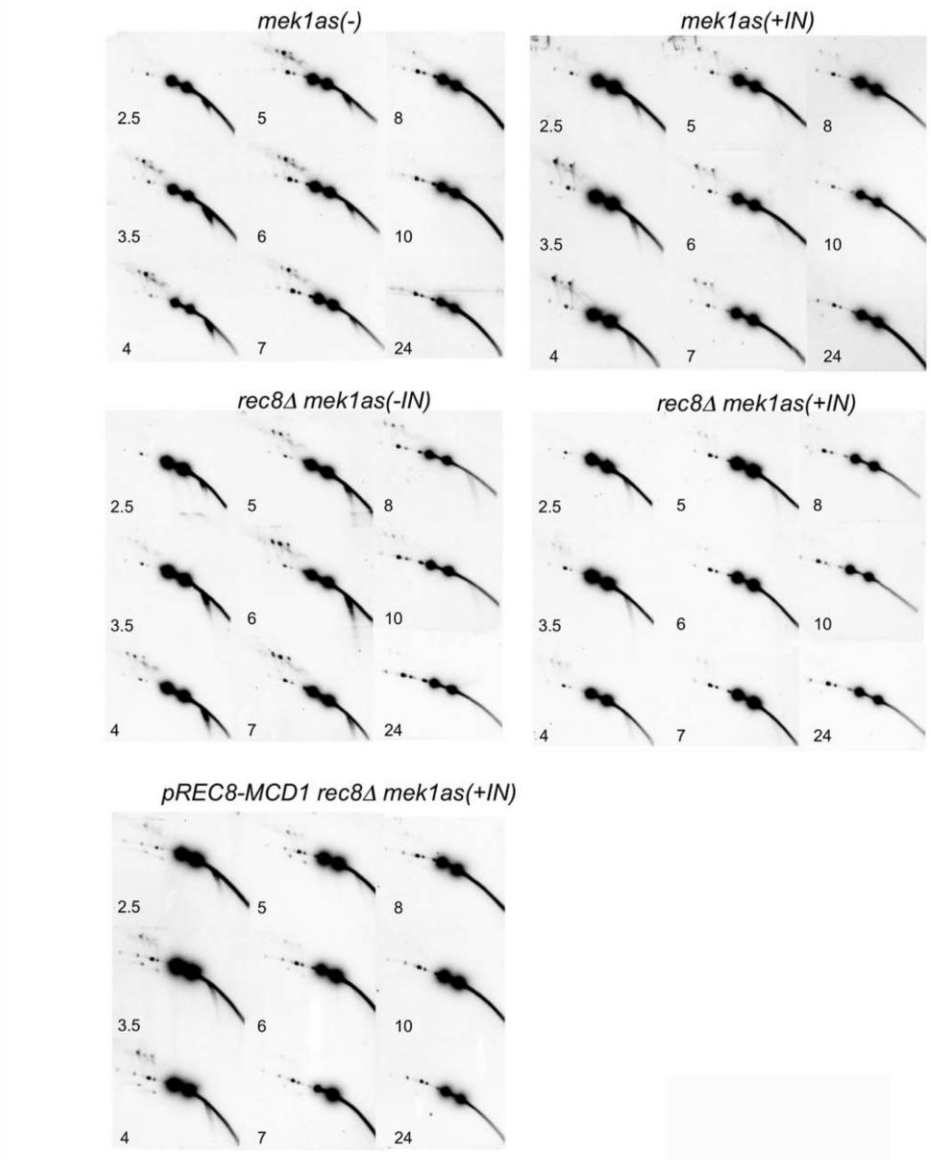

Figure S2. Two-dimensional gel images for *mek1as* data set. Related to Figures 4 and 5. Images of 2D gel Southern analysis showing DNA species from representative meiotic time course. Species as detailed in Figures 2D and 5ABC.

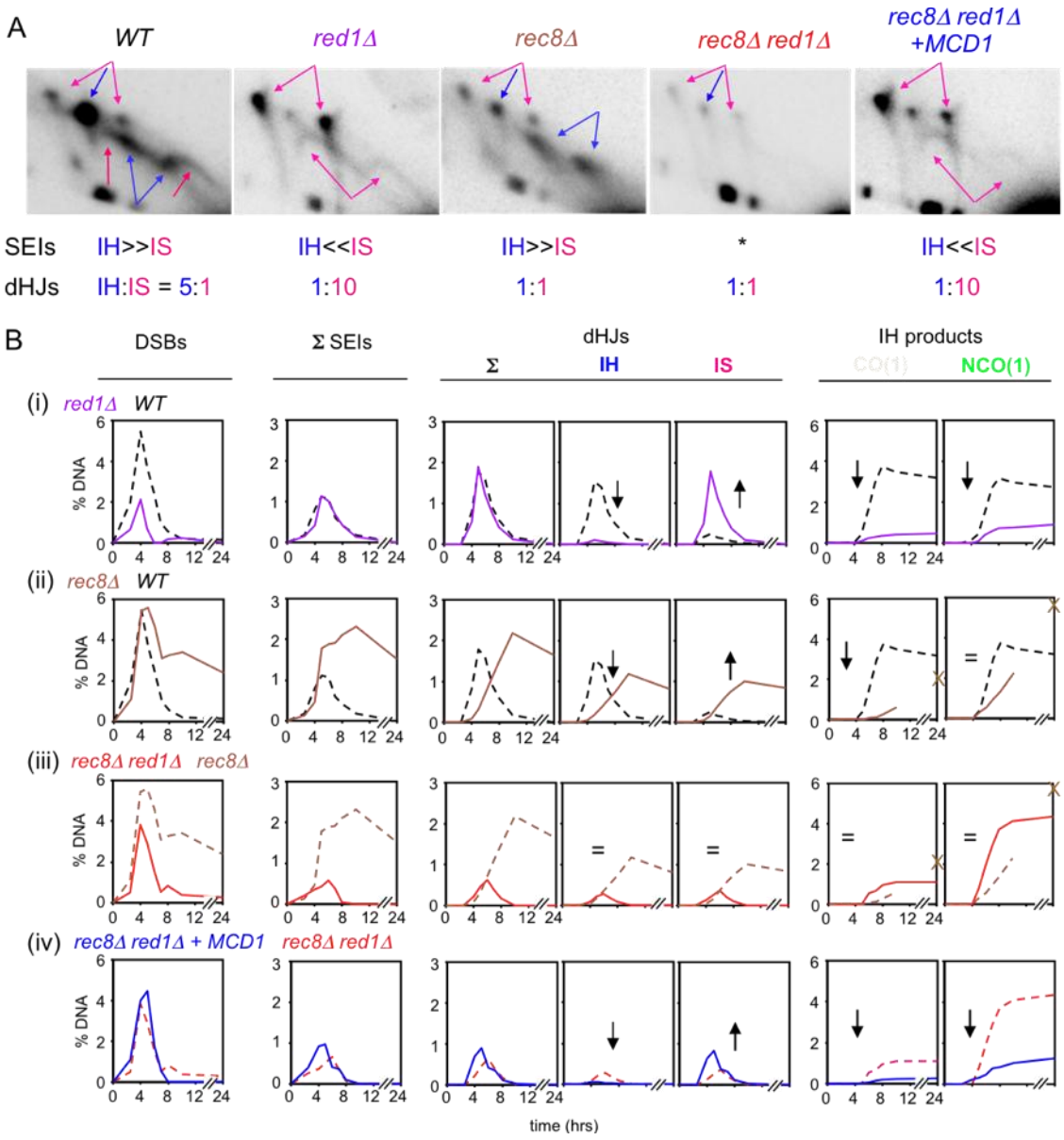

Figure S3. Recombination patterns in *MEK1* ± *red1Δ* strains. Related to Figure 4. Data analogous to Figure 4ABD for *MEK1*± *red1Δ* versions of the five strain phenotypes. (A) Representative 2D gel from WT and each of the four indicated mutant strains at the time point when SEIs and dHJs are at their maximum levels. Identical patterns are observed as for the corresponding *mek1as* strains (Figure 4A). (B) Quantification of recombination intermediates in *MEK1*± *red1Δ* versions of all five strains exactly as in Figure 4D. Patterns are

the same as those observed for the corresponding *MEK1+ red1Δ* strains (Figure 4D). For *rec8Δ*, IH-CO and IH-NCO levels at t=24h indicated by "X". IH:IS dHJ comparisons for these *MEK1+ red1Δ* strains are shown in parallel with comparisons for *mek1as* strains in Figure 4B.

Note re progression of recombination in Rec8- strains. Previous studies asserted that a *rec8Δ* strain exhibits a strong block to execution of recombination, as indicated by accumulation of DSBs to higher than normal levels at later than normal times and, in one study, a severe defect in formation of COs (Klein et al, 1999; Brar et al, 2009; Callender and Hollingsworth, 2010). Neither of these assertions is borne out by the further studies presented here. The reported defect in IH-CO formation was four-fold (Brar et al, 2009) but did not take into account a reduction in DSB levels; we show here that DSBs are reduced two-fold and IH-COs are reduced to ~60% the WT level due to a homolog bias defect. These effects together account for the previously reported four-fold reduction. Further, they imply that the majority of DSBs progress to products. Efficient progression of DSBs to products in *rec8Δ* is also documented by additional findings. (1) DSBs, SEIs and dHJs do occur at higher than normal levels at later than normal times; however, by t=24h, the absolute fraction of initiated interactions represented by these species is very low, each representing less than 20% of initiated interactions at all temperatures. (2) IH-NCOs occur at high, WT-like levels while IH-COs occur at a reduced level explained by altered homolog bias (above). (3) In one prior study (Klein et al., 1999), unusually high absolute levels of DSBs were observed at "normal" times because of a defect in execution of Southern blotting, apparent by inspection of

the published data: insufficient denaturation leads to differential hybridization of DSBs due to the single-stranded character of their 3' ssDNA tails. Extraordinarily high levels of DSBs were seen in both WT and *rec8Δ* strains in the presented data; however, the relative abundance of DSBs in *rec8Δ* vs WT was very similar to that observed here. However, there are likely a few DSBs that stall for an especially significant period of time. A few extra IS-SEIs arise at very late times, accompanied by the characteristic appearance of DSB resection, but do not progress specifically to IS-dHJs (K.K. unpublished).

We also note that in *rec8Δ mek1as(-IN),* DSBs, SEIs and dHJs appear and disappear in a relatively timely fashion and with very low levels remaining at late times (t=12- 24h) (Figures 4D, 5D, S2). In both Rec8- Mek1kinase- strains, progression is also efficient and is even faster than in *rec8Δ mek1as(-IN)* due to the effects of Red1/Mek1kinase on progression (text). Thus, the *mek1as(-IN)* allele is a hypomorph for control of progression in *rec8Δ*, even though it has no discernible effect on recombination in an otherwise WT strain (text).

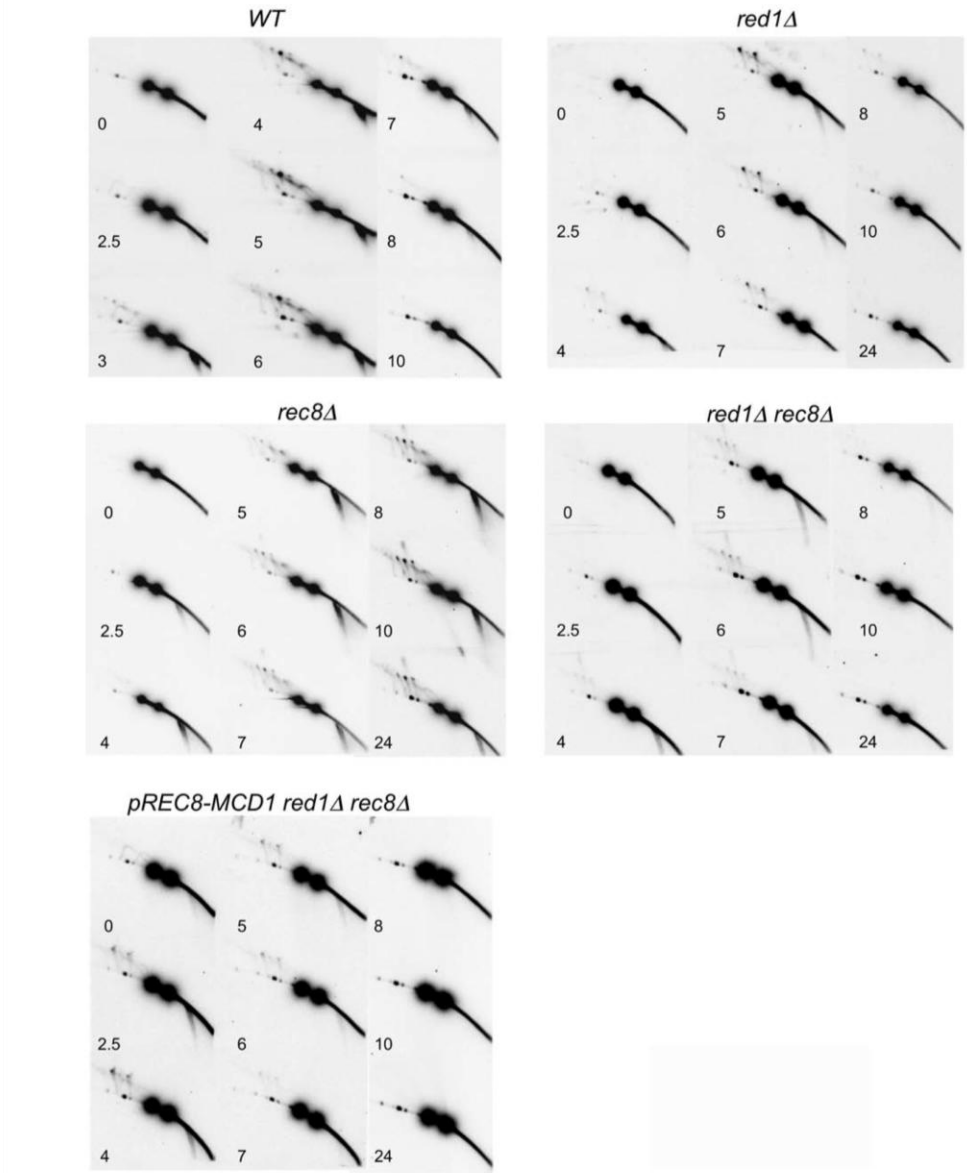

Figure S4. Two-dimensional gel images for *MEK1* ± *red1Δ* data set.

Related to Figures 4 and 5. Images of 2D gel Southern analysis showing DNA species from representative meiotic time course. Species as detailed in Figures 2D and 5ABC.

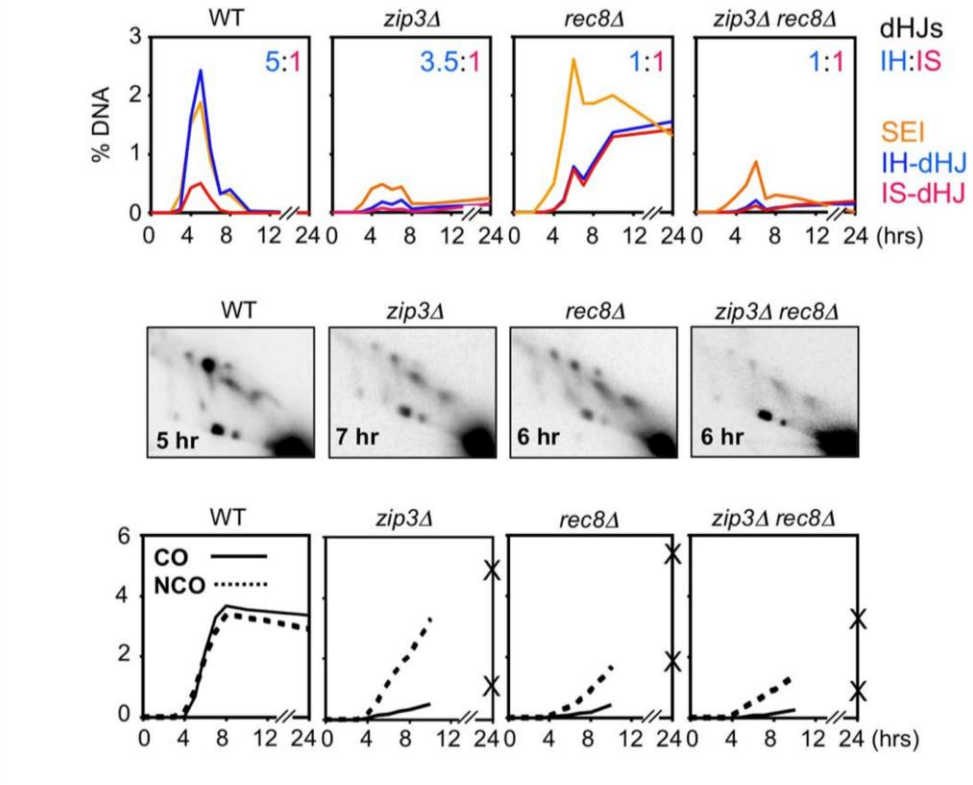

Figure S5. Functional relationships between Zip3 and Rec8. Related Figures 4 and 5. **(A)** For the four indicated strains (± Zip3 ± Rec8), absolute levels of SEIs and IH- and IS-dHJs are compared exactly as in Figure 4D. **(B)** Corresponding gels for the strains in (A) taken from the time point where SEIs/dHJs are maximally abundant as indicated. These gels illustrate the fact that all CO-related species (IH/IS dHJs and IS-SEIs as well as IH-SEIs) co-vary in abundance in all strains over time. More specifically: there is no indication that patterns in the "SEI region" of the gel are significantly different among the four strains, at any time point, as illustrated for one time point here. **(C)** IH-CO and IH-NCO levels over time in the four indicated strains (± Zip3 ± Rec8). Levels at t=24h indicated by "X".

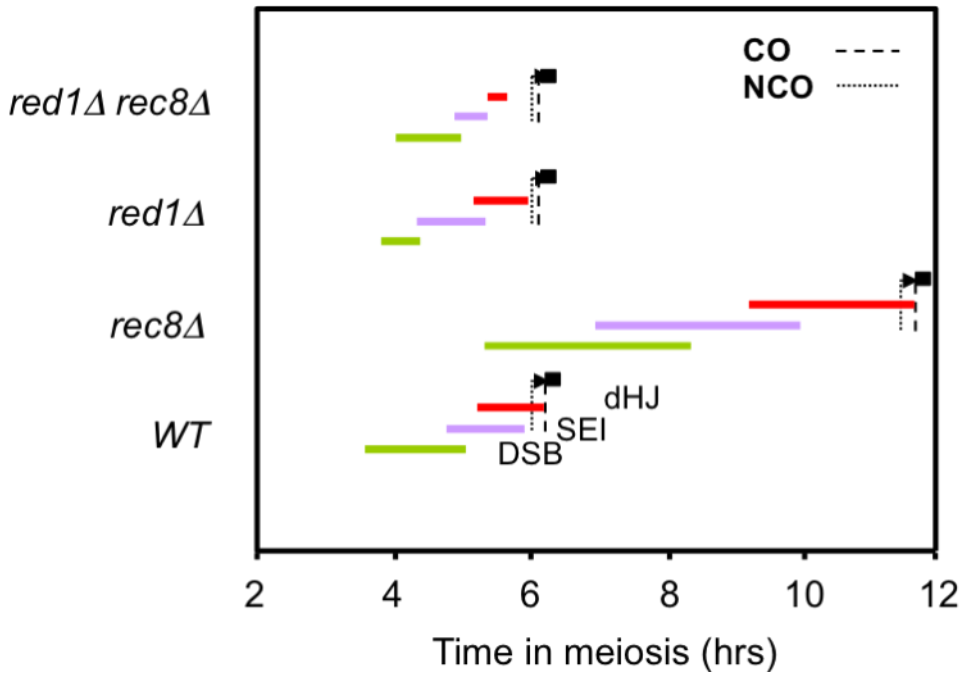

Figure S6. Timing and kinetics of recombination. Related Figure 5.

Progression phenotypes of strains of the *MEK1* ± *red1Δ* data set (Figure 4B, Figures S3, S4) determined identically to those for the *mek1as* data set as described in Figure 5D.

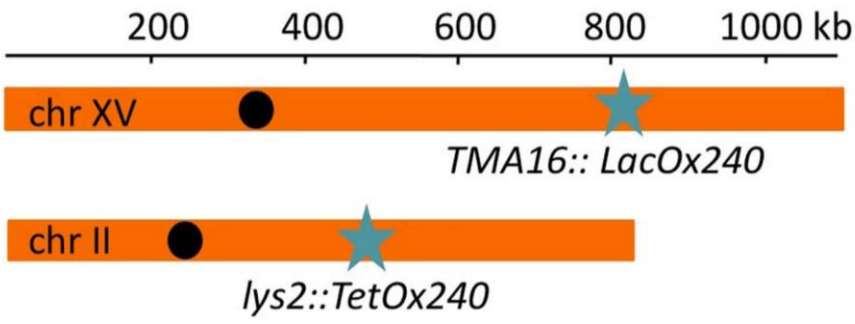

Figure S7. Diagram of chromosomal location of *tet* and *lac* operator arrays. Related to Figure 6. The arrays are denoted by stars. Black circles represent centromeres.

Extended Experimental Procedures

Strains. Recombination strains: WT (NKY3738), *rec8Δ* (NKY3739), *red1Δ* (NKY4006), *red1Δ rec8Δ* (NKY4007), *zip3Δ* (NKY3742), *rec8Δ zip3Δ* (NKY3775), *rad50S* (NKY3740), *rec8Δ rad50S* (NKY3741), *red1Δ rad50S* (NKY4009), *red1Δ rec8Δ rad50S* (NKY4008), *mek1Δ mek1as* (NKY4038), *rec8Δ mek1Δ mek1as* (NKY4035), *pRec8-MCD1::rec8Δ* (NKY3966), *pRec8-MCD1:: red1Δ rec8Δ* (NKY3967), and *pRec8-MCD1::rec8Δ mek1Δ mek1as* (NKY4048). Cytological analysis utilized the following strains: *REC8-myc13/REC8, PDS5-GFP/PDS5* (NKY3878*); lys2::TetOx240:URA3/+, leu2::LEU2- tetR-GFP* (NKY3747*); rec8Δ, lys2::TetOx240:URA3/+, leu2::LEU2- tetR-GFP* (NKY3870); *red1Δ, lys2::TetOx240:URA3/+, leu2::LEU2- tetR-GFP* (NKY3922); *rec8Δ, red1Δ, lys2::TetOx240:URA3/+, leu2::LEU2- tetR-GFP/leu2* (NKY3925); *URA3::CYC1p-LacI-GFP/ ura3∆, TMA16:: LacOx240:URA3/+* (NKY3840); *rec8Δ, URA3::CYC1p-LacI-GFP/ ura3∆, TMA16:: LacOx240:URA3/+* (NKY3928); *rec8Δ, leu2::URA3p-tetR-tdTomato::LEU2/leu2, lys2::TetOx240:URA3/+, URA3::CYC1p-LacI-GFP/", TMA16::LacOx240:URA3/+* (NKY4059).

Time courses. Two different presporulation regimes were used in these experiments, using either SPS or YPA for presporulation medium (Koszul et al., 2009: Weiner and Kleckner, 2009). The two methods give very similar results with respect to the timing of all assayed events (DNA replication, DNA events of recombination, MI and MII divisions and spore formation).

Both regimes start similarly from glycerol stocks maintained at -80°C. Preliminary steps are all performed at 30°C. Strains are patched onto YEPG plates (3% w/v glycerol, 2% w/v bactopeptone, 1% w/v yeast extract, 2% w/v bactoagar) overnight. Cell are then struck out to single colonies on YEPD plates (2% w/v bactopeptone, 1% w/v yeast extract, 2% w/v glucose, 2% w/v bactoagar) and grown for three days. A single colony is transferred to 5 ml YEPD liquid medium (2% w/v bactopeptone, 1% w/v yeast extract, 2% w/v glucose) and grown overnight.

For SPS cultures a 1/1000 dilution of the culture is made using SPS medium (1% w/v potassium acetate, 1% w/v bactopeptone, 0.5% w/v yeast extract, 0.17% w/v yeast nitrogen base with ammonium sulfate and without amino acids, 0.5% w/v ammonium sulfate, 0.05M potassium biphtalate, 2 drops per liter antifoam (Sigma), pH to 5.5 with 10 N KOH) and grown for 18 hrs. Meiosis was initiated by transfer of cells to 1% SPM (1% w/v potassium acetate, 0.02% w/v raffinose, 2 drops per liter antifoam).

For YPA cultures a 1/200 dilution of the culture was made using YEPA medium (1% w/v potassium acetate, 2% w/v bactopeptone, 1% w/v yeast extract, 2 drops per liter antifoam) and grown for 13.5 hrs. Meiosis was initiated by transfer of cells to 0.3% SPM (0.3% w/v potassium acetate, 0.02% w/v raffinose, 2 drops per liter antifoam).

For 33°C analysis, using either regime, cells were kept at 30°C through t = 2.5 hours with shift to 33°C occurring thereafter (for rationale, see Börner et al., 2004). For analysis of mutants containing *mek1as*, a single SPS culture was synchronized and divided into two identical sporulation cultures then in one of the two cultures, Mek1 kinase activity was inhibited by addition of fresh 1 μM 1-NA-PP1 (USBiological) (Nui et al., 2005).

DNA Physical Assays. Chromosomal DNA preparation and physical analysis were performed as described previously (Schwacha and Kleckner, 1994; Hunter and Kleckner, 2001). Genomic DNA (2 µg) was digested with 80 units XhoI (New England Biolabs), and precipitated. DNA pellets were dissolved in DNA loading buffer and electrophoresis of one-dimensional gel (0.6% agarose gel in TBE [89 mM Trisborate, 2 mM EDTA, pH 8.3]) was carried out in TBE buffer at ~2V/cM for 24hr. Two-dimensional gel electrophoresis was performed as described (Allers and Lichten, 2001; Schwacha and Kleckner, 1994) with the following modified procedures. About 2 µg of XhoI-digested DNA was loaded onto 0.4% Seakem Gold agarose gel lacking ethidium bromide in TBE. Gel electrophoresis was carried out at ~1V/cM for 20 hr at room temperature. Gels were stained in TBE containing 0.5 µg/ml ethidium bromide, and slices of lanes were cut to cover the DNA of interest. The gel slices containing the lane were placed on the 2D apparatus gel tray at 90° degree to the direction of electrophoresis. DNA was placed so that the higher molecular weights were to the left. Second dimensional gel (0.8% agarose gel in TBE containing 0.5 µg/ml ethidium bromide) was poured around the gel slices and allowed to solidify. Electrophoresis in the second dimensional gel was performed in pre-chilled TBE containing ethidium bromide at ~6V/cm for 5 hrs at 4°C. For CO/NCO assays, DNA (2 µg) digested with both XhoI and NgoMIV was analyzed on 1D gel electrophoresis as shown in above. Gels were subjected to Southern blot analysis after transfer onto Zeta-Probe GT membranes (Bio-Rad). Probes were radiolabeled using a Stratagene RmT Random Priming kit. Hybridizing DNA species are quantified using a Bio-Rad phosphoimager with QuantityOne software.

Quantification and reproducibility of DNA signals in 1D and 2D gels. Southern blots were analyzed using a Biorad Molecular phosphorimager FX in combination with quantification using Quantity One software from Bio-rad. Phosphorimager analysis of the blots directly detects the intensity of the signal over a wide dynamic range. This approach avoids complications that arise by quanitification of signals from indirect readouts. TIFF/JPEG/BMP images do not encompass the full dynamic range of the phosphorimager so are subject to “saturation” of signal intensity. This leads to underestimation of the levels of more intense signals relative to less intense signals and thus inaccuracies in quantification of relative signal intensities (e.g. IH:IS dHJ ratios). More specifically, we have performed reconstruction experiments to demonstrate that analyzing TIFF images generated from scanner data e.g. those presented in Figure 3, leads to inaccurate IH:IS dHJ ratios. In addition, analysis of raw phosphorimager data means that quantifications presented are accurate irrespective of whether the images presented for publication are, or are not, overexposed.

Another issue of importance for determination of IH:IS dHJ ratios is that it is essential to compare IH-dHJ levels to the sum of the IS-dHJ levels from the two parents. This is for two reasons. First, IH-dHJs arise from DSBs on both homologs and thus must be compared to IS-dHJs that arise from DSBs on both homologs. Second, it is not appropriate to simply analyze the level of IS-dHJs from one homolog and double that number because the two homologs exhibit different levels of DSBs at the HIS4LEU2 locus. This is true not only for earlier HIS4LEU2 alleles, where the difference is very obvious, but in the current allele. This is not a point that is normally emphasized. However, it is nonetheless true and is visible from data presented in other studies, e.g. from the Hunter laboratory (Oh et al., 2007; Lao et al., 2008). DSBs are

less abundant for the “Dad” homolog than for the “Mom” homolog. Thus, if only the DAD/DAD IS-dHJ signal is used, the IH:IS ratio will be too high while, if only the Mom/Mom IS-dHJ signal is used, the IH:IS ratio will be too low. We also note that, using this approach, an IH:IS dHJ ratio of 1:1 ratio is observed even from an old version of the HIS4LEU2 locus (Mlu/Bam) where the DSB levels for the two homologs differ by two-fold (Xu and Kleckner, 1995).

Predictions of two models for IH-CO reductions in Rec8- strains. WT IHI:IS ratio = 5:1 implies 6x SEIs total with 5x going to IH-dHJs and 1x going to IS-dHJs. Loss of IH-SEIs would imply 1x going to IS-dHJs and 1x going to IH-dHJs, giving 1:1 IH:IS dHJ ratio; reduction in IH-dHJs from 5x to 1x would then give 20% the WT level of IH-COs. Loss of bias would imply 3x SEIs going to 3x IH-dHJs and 3x SEIs going to IS-dHJs, giving 1:1 IH:IS dHJ ratio; reduction in IH-dHJs from 5x to 3x would then give 60% the WT level of IH-COs.

Analysis of sister cohesion. At time points indicated aliquots were removed for analysis. Samples for FACS, sister cohesion, and divisions were fixed in 40% ethanol, 0.1 M sorbitol then stored at -20°C. FACS analysis was essentially as described in Cha et al., 2000 except that 5 µM Sytox Green (Molecular Probes) was used to specifically stain DNA rather than propidium iodide. Fixed cells were transferred to 50 mM Tris pH 7.5 and 100 µg/ml RNase then incubated overnight at room temperature. The fraction of cells in the 4C peak was quantitated using Image J (NIH) software. Meiotic divisions were monitored by staining with 1 µg/ml DAPI (4’, 6-diamidino-2-phenylindole) (Padmore et al., 1991). For cohesion analysis cells were spun down then resuspended in 10 mM Tris, pH 8.0, 1 µg/ml DAPI and visualized immediately on an Axioplan IEmot

microscope (Zeiss) using Metamorph (Molecular Devices) image acquisition and analysis software using appropriate filters for GFP and dTomato. To calculate the percentages predicted for independent loss of cohesion at the two loci the percentages of cells exhibiting separation at each locus were considered individually, then at each time point the binomial distribution: [% both = (%lac)(%tet)] and [% neither = (1-%lac)(1-%tet)], was used to derive the predicted result. It was assumed that 5% of cells fail to enter meiosis under these conditions (Padmore et al., 1991).

Immunocytology. Chromosome spreads were prepared essentially as described in Loidl et al., 1998. Cells were harvested at hourly intervals then spheroplasted to remove the cell wall. They then were resuspended in MES wash (1 M sorbitol, 0.1 M MES, 1 mM EDTA, 0.5 mM $MgCl_2$ pH 6.5). Lysis and spreading were achieved by placing on a slide, cell suspension, fixative (3% w/v paraformaldehyde, 3.4% w/v sucrose), detergent (1% Lipsol- LIP Ltd., Shipley England), then after 1 min, more fixative in the ratio of 1:2:4:4. Immunofluorescent labeling was performed according to Bishop, 1994. Slides were incubated at room temperature in TBS buffer (25 mM Tris-Cl, pH 8, 136 mM NaCl, 3 mM KCl) then blocked with TBS buffer-1% w/v Bovine serum albumin (BSA). Primary antibodies, mouse monoclonal anti-myc, goat polyclonal anti-Zip1 (Santa Cruz) or rabbit polyclonal anti-Red1, were diluted appropriately in TBS- 1% BSA. Secondary antibodies were anti-mouse, anti-goat, or anti-rabbit IgG labeled with Alexa488 or Alexa594 (Molecular Probes), or Cy5 (Amersham) and diluted appropriately in TBS- 1% BSA. Slides were stained with 1 µg/ml DAPI and mounted in Slow Fade Light (Molecular Probes). Spread chromosomes were visualized on an

Axioplan IEmot microscope (Zeiss) using appropriate filters. Images were collected using Metamorph (Molecular Devices) image acquisition and analysis software.

Supplemental References

Allers, T., and Lichten, M. (2001). Differential timing and control of noncrossover and crossover recombination during meiosis. Cell *106*, 47-57.

Brar, G.A., Hochwagen, A., Ee, L.S., and Amon, A. (2009). The multiple roles of cohesin in meiotic chromosome morphogenesis and pairing. Mol. Biol. Cell *20*, 1030-1047.

Koszul, R., Kameoka, S., and Weiner, B.M. (2009). Real-time imaging of meiotic chromosomes in Saccharomyces cerevisiae. Methods Mol. Biol. *558*, 81-89.

Loidl, J., Klein, F., and Engebrecht, J. (1998). Genetic and morphological approaches for the analysis of meiotic chromosomes in yeast. in Meth. Cell Biol. Vol. 53, M. Berrios, ed. (Academic Press, San Diego, CA), pp. 257-285.

Weiner, B.M., and Kleckner, N. (2009). Assaying chromosome pairing by FISH analysis of spread *Saccharomyces cerevisiae* nuclei. Methods Mol. Biol. *558*, 37-51.

Xu, L., and Kleckner, N. (1995). Sequence non-specific double-strand breaks and interhomolog interactions prior to double-strand break formation at a meiotic recombination hot spot in yeast. EMBO J. *14*, 5115-5128.

Supplemental Figure 1

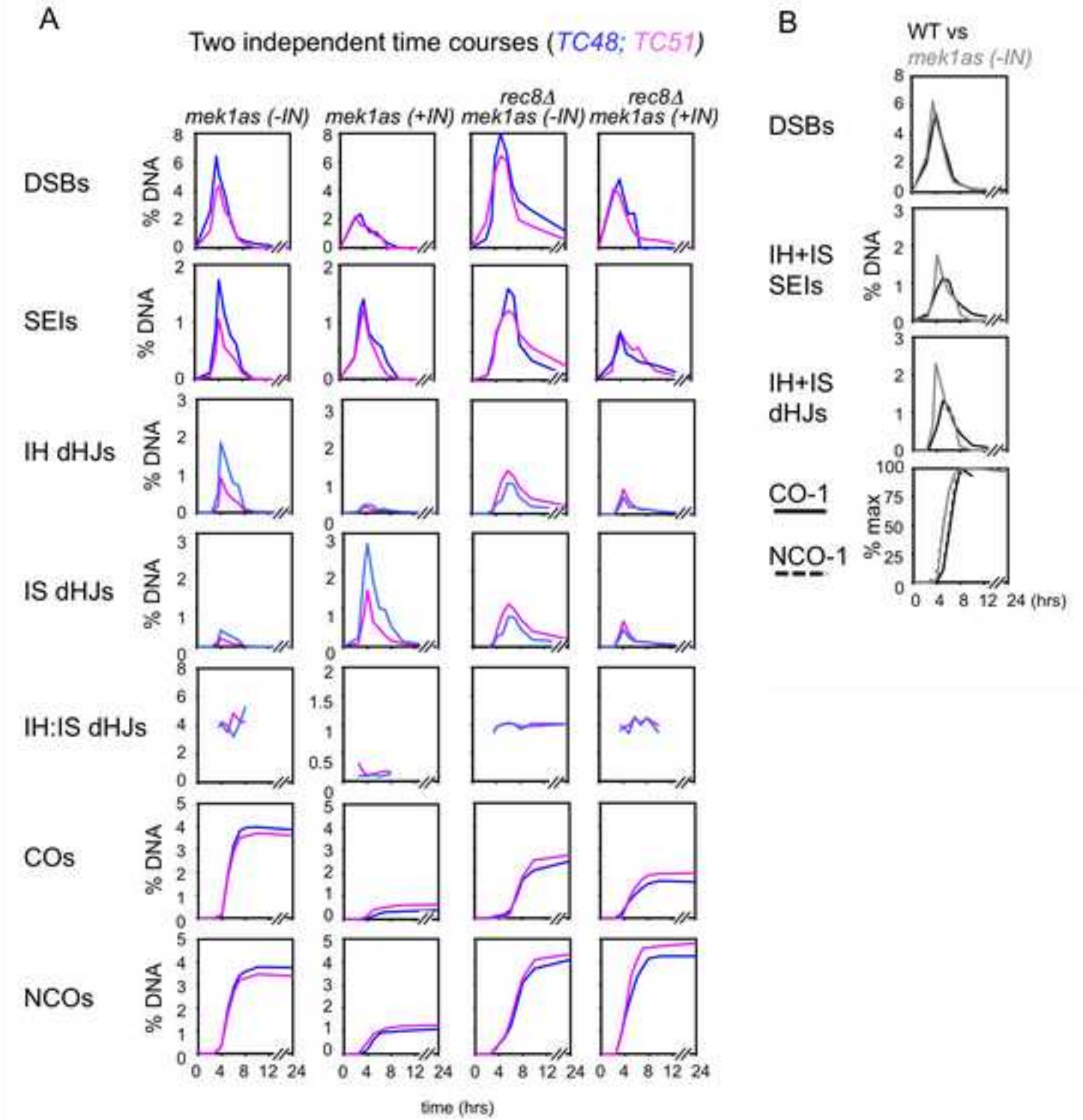

Supplemental Figure 2

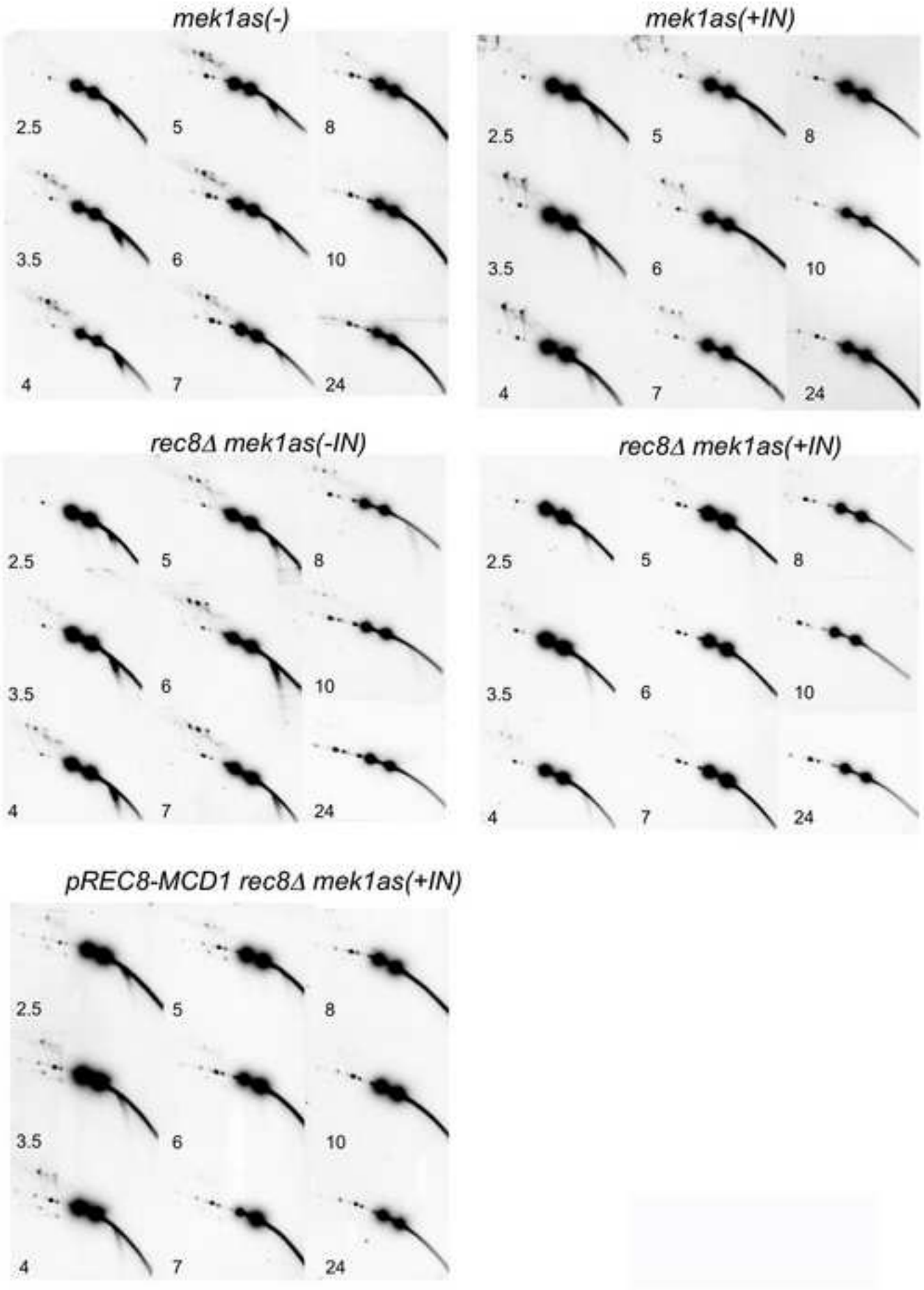

Supplemental Figure 3

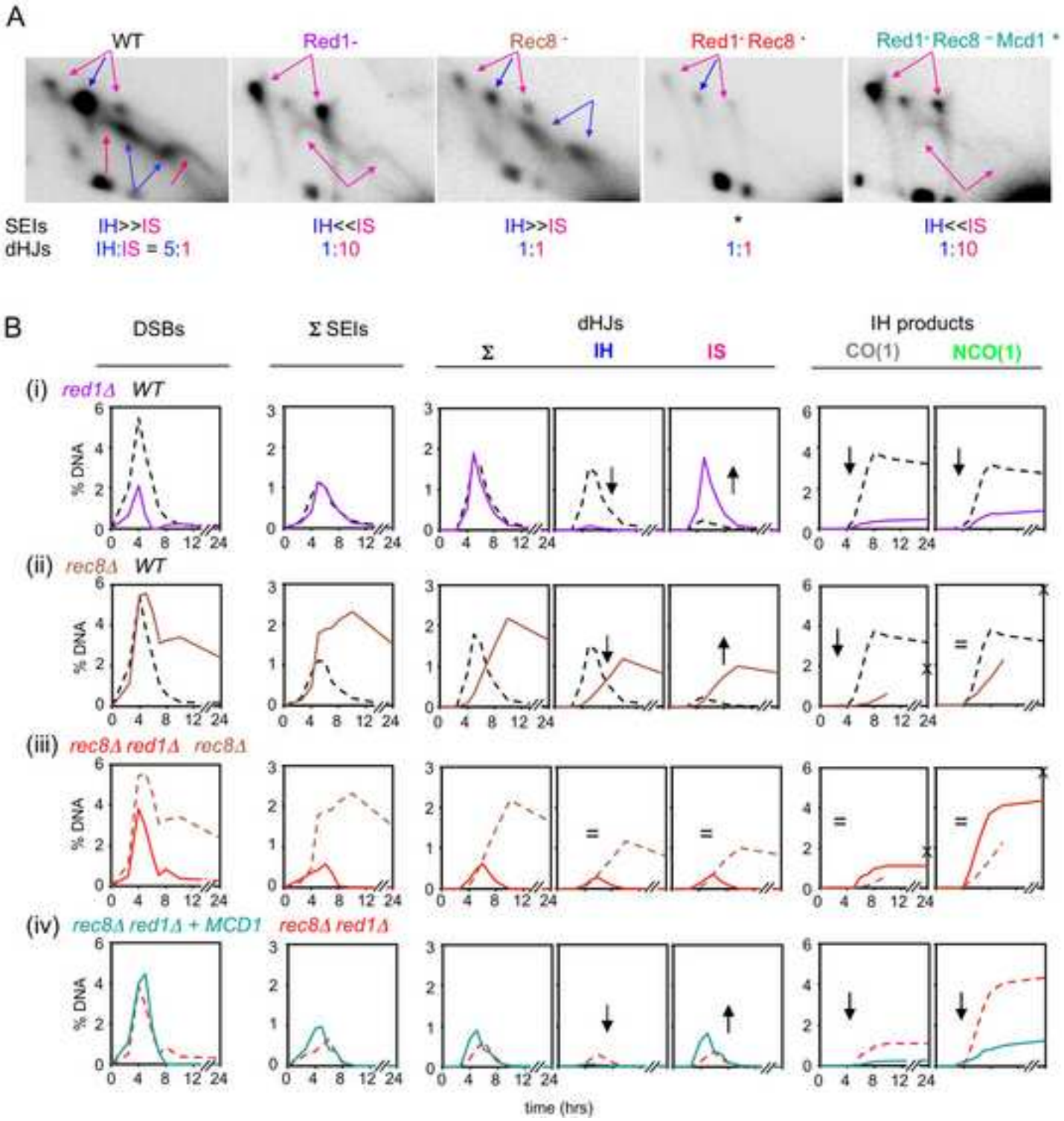

Supplemental Figure 4

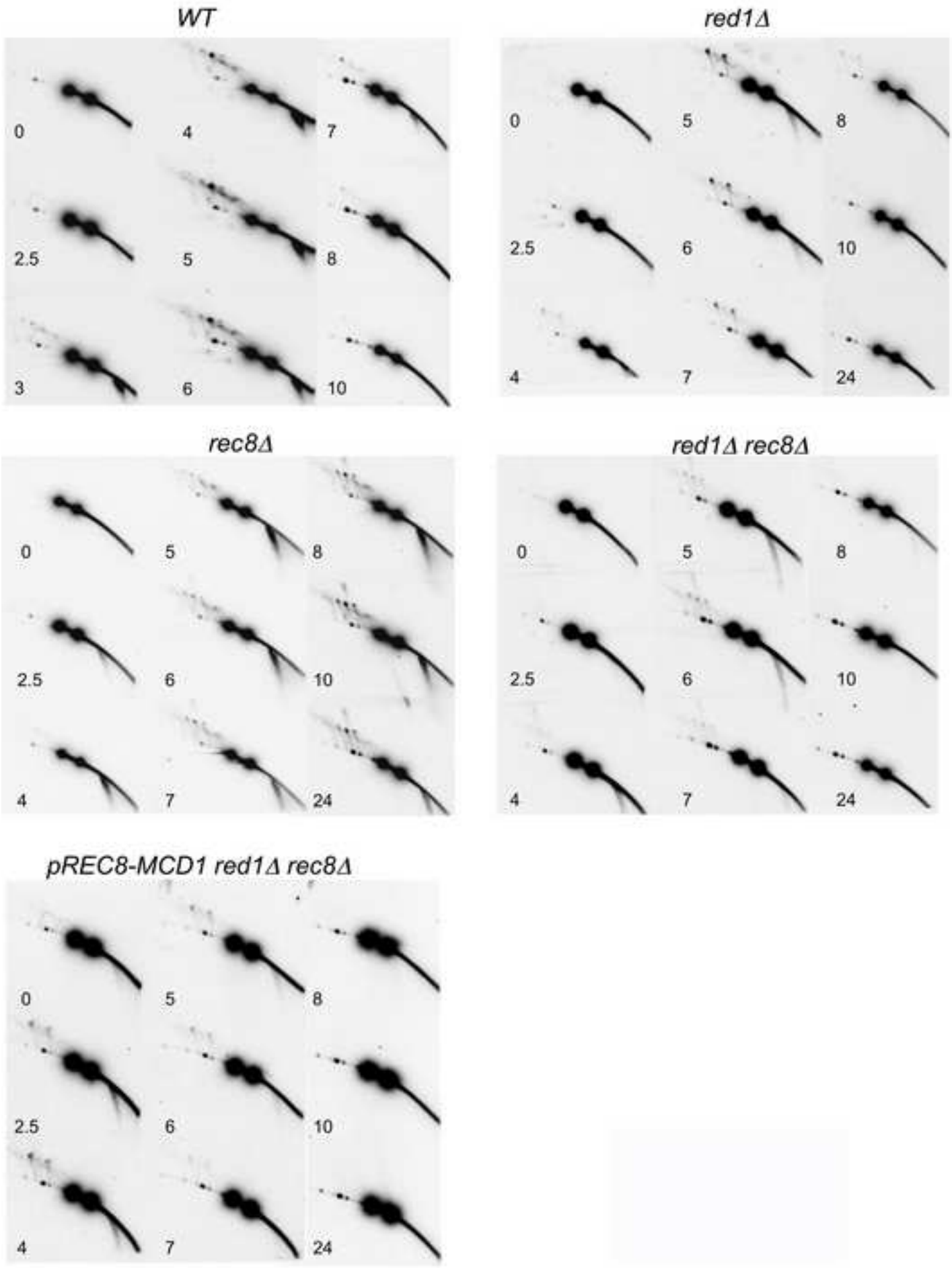

Supplemental Figure 5

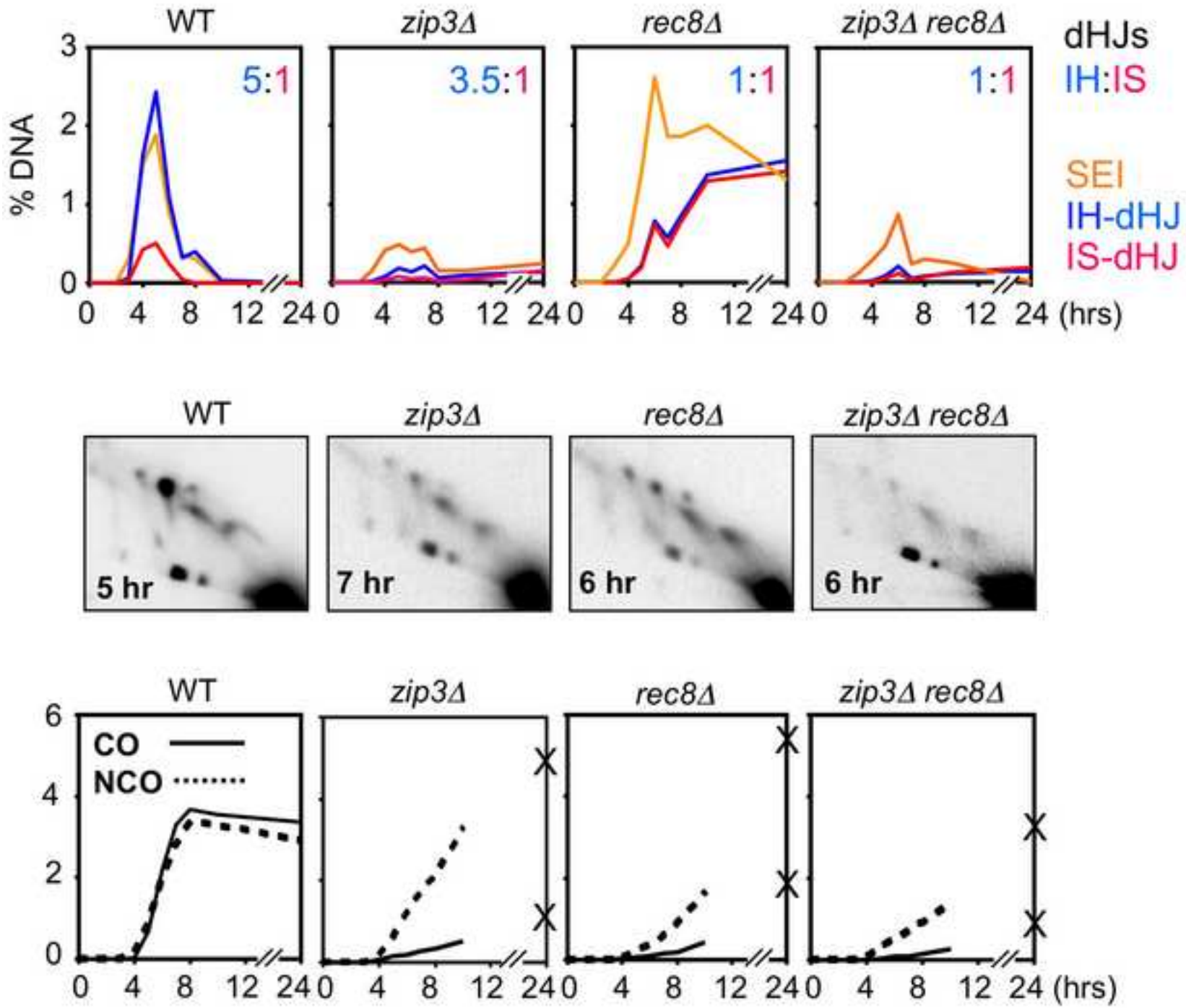

Supplemental Figure 6

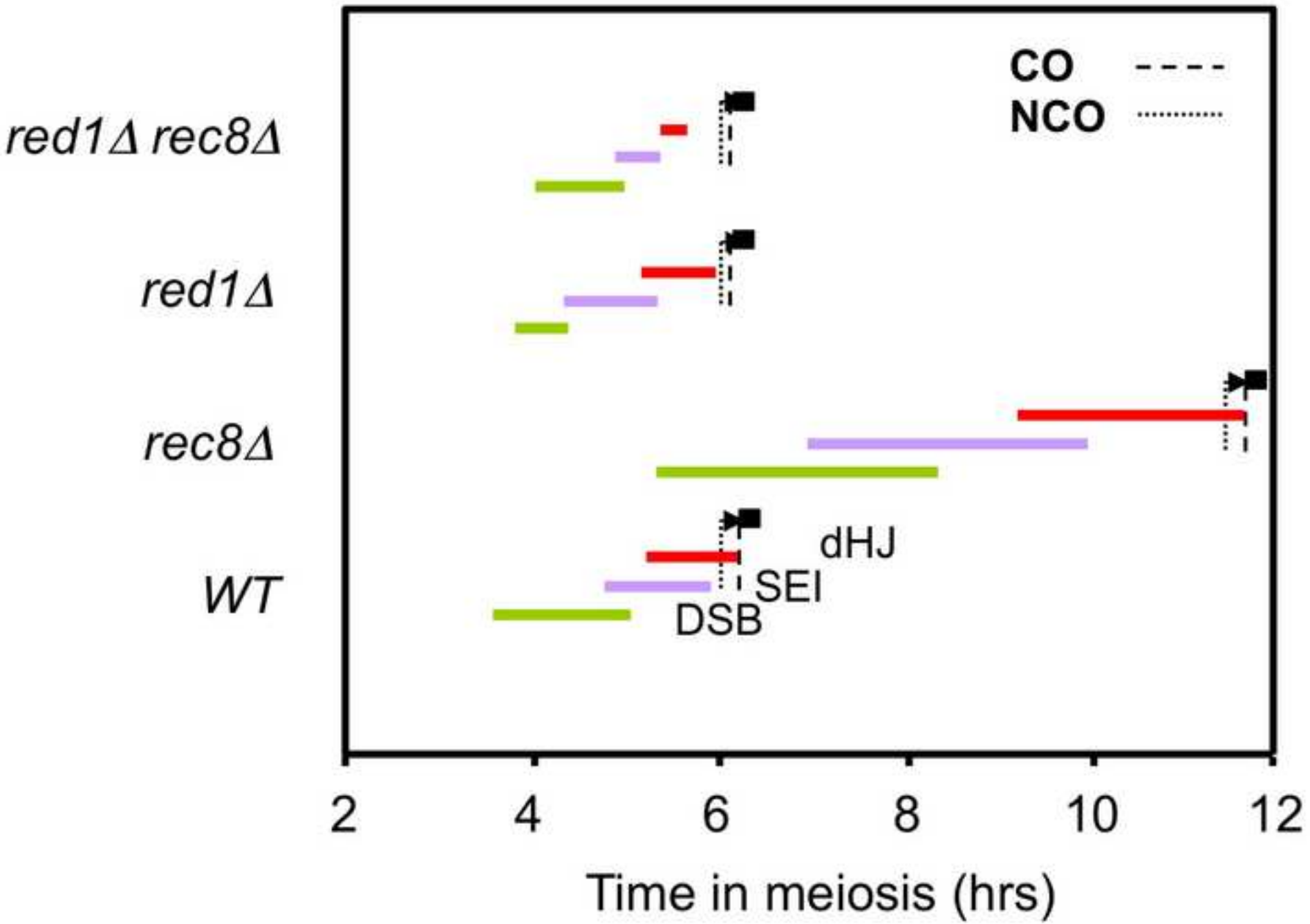

Supplemental Figure 7